의학박사 학위 논문

Feasibility study of real-time in vivo cell trafficking using ^{89}Zr-DFO labeled CAR T-cell PET imaging

^{89}Zr-DFO 표지 CAR-T 세포 영상을 이용한 실시간 체내 세포 추적 가능성 연구

울 산 대 학 교 대 학 원

의 학 과

이 석 현

Feasibility study of real-time in vivo cell trafficking using ^{89}Zr-DFO labeled CAR T-cell PET imaging

지 도 교 수　　류 진 숙

이 논문을 의학박사 학위 논문으로 제출함

2018년 12월

울 산 대 학 교　대 학 원

의 학 과

이 석 현

이석현의 의학박사 학위 논문을 인준함

심사위원 김 재 승 (인)
심사위원 류 진 숙 (인)
심사위원 오 승 준 (인)
심사위원 김 석 영 (인)
심사위원 이 상 진 (인)

울 산 대 학 교 대 학 원

2018년 12월

Abstract

Background: Chimeric antigen receptor (CAR) T-cells have been developed in recent years, producing impressive clinical reports in patients with hematologic malignancies. However, there is no standardized method available for cell trafficking and monitoring of the *in vivo* behaviors of injected CAR T-cells. This study aimed to assess the feasibility of real-time *in vivo* ^{89}Zr-p-Isothiocyanatobenzyl-desferrioxamine B (Df-Bz-NCS, DFO) labeled CAR T-cell trafficking using positron emission tomography (PET).

Methods: After synthesizing ^{89}Zr-DFO, 74 ~ 185 kBq/10^6 cells were used for radiolabeling Jurkat cells stably expressing CD19-targeting CAR (Jurkat/CAR T-cells) and T cells obtained from human peripheral blood mononuclear cells (hPBMC). Cell labeling efficiency was obtained and after labeling cells with ^{89}Zr-DFO, cell viability, proliferative activity and cytokine IL-2 or IFN-γ production as functional indexes were compared with unlabeled cells in *in vitro* settings. Bilateral xenograft model bearing Raji (CD19 positive) and K562 (CD19 negative) tumors was established, and serial PET/magnetic resonance (MR) images were acquired until day 7 after injection of ^{89}Zr-DFO labeled Jurkat/CAR T-cells or hPBMC CAR T-cells. All images were quantitatively analyzed. Immediately after 7-day imaging of Jurkat/CAR T-cells, the mice were sacrificed, and the radioactivity from the harvested mouse tissues including lung, liver and spleen were counted by gamma counter for the evaluation of *ex vivo* biodistribution. The distributions of injected unlabeled Jurkat/CAR T-cells on 3 days after injection were also separately cross-confirmed using flow cytometry, Alu-PCR and immunohistochemistry (IHC).

Results: The ^{89}Zr-DFO radiolabeling efficiency of Jurkat/CAR and hPBMC CAR T-cells was 70 ~ 79%, and cell radiolabeling activity was 98.1 ~ 103.6 kBq/10^6 cells. Cell viability after radiolabeling was >95%. Compared with unlabeled cells, there was no significant difference in cell proliferation during the early period after injection; however, the proliferative capacity decreased over time (p = 0.02, day 7 after labeling). There was no significant difference in IL-2 or IFN-γ secretion between unlabeled and labeled CAR T-cells. PET/MR images in the xenograft model showed that most of the ^{89}Zr-labeled Jurkat/CAR T-cells were distributed in the lung (25.0% ± 3.7%ID[injected dose]) and liver (23.4% ± 5.3%ID) by 1 hour after injection. The cells gradually migrated to the liver by day 1, where they remained stable until day 7 (on day 7: lung 3.9% ± 1.0 %ID, liver 35.7% ± 1.0 %ID, spleen

1.4% ± 0.4 %ID). No significant accumulation of labeled cells was identified in tumors. A similar pattern was observed in *ex vivo* biodistributions on day 7 (lung 3.0% ± 1.0%ID, liver 19.8% ± 2.2%ID, spleen 2.3% ± 1.7%ID). Similarly, the tracing of ^{89}Zr-labeled hPBMC CAR T-cells showed the same pattern on serial PET images as Jurkat/CAR T-cells. The distribution of CAR T-cells was also confirmed by flow cytometry, Alu polymerase chain reaction, and immunohistochemistry.

Conclusions: The feasibility of CAR T-cells trafficking *in vivo* using serial PET imaging after administration of ^{89}Zr-DFO labeling was confirmed. The results suggest that PET imaging of CAR T-cells, labeled with ^{89}Zr-DFO, can be used to investigate cellular kinetics, initial *in vivo* biodistribution, and the safety profile of future CAR T-cell development.

Keywords: Chimeric antigen receptor (CAR) T-cell, cell trafficking, p-Isothiocyanatobenzyl-desferrioxamine B (Df-Bz-NCS, DFO), positron emission tomography (PET)

Contents

List of Tables and Figures

Introduction

Given shifting cancer treatment paradigms, chimeric antigen receptor (CAR) T-cell immunotherapy has developed very rapidly [1, 2]. CAR T-cells, which have been studied as immune regulatory cell therapies, harbor fusion proteins with the extracellular scFv domain of an antibody. These proteins recognize the characteristic antigen on the cancer cell surface and the intracellular co-stimulatory domain for T-cell activation. When CAR T-cells grab the antigen on the surface of the tumor cell, a sequential co-stimulatory signal activates the T-cell and triggers the signaling pathway within the cell, thereby allowing the CAR T-cells to kill the tumor cell [3, 4]. Moreover, because of its continuous tumor cell-killing activity, CAR T-cells are a "living drug" that can proliferate in the body and kill tumor cells. They have a significantly longer action than conventional chemotherapeutics and antibody drugs [5]. CAR T-cell therapy has shown dramatic anti-cancer effects, particularly in clinical trials for patients with hematological malignancies such as refractory B-cell malignancies, after standard treatment [6-8].

Despite its successful use in patients with B-cell malignancies, there is a lack of substantive understanding of CAR T-cells in the human body: 1) a limited effect of CAR T-cells on solid tumors, 2) the trafficking and biodistribution of CAR T-cells, and 3) the targeting efficacy of CAR T-cells that are injected within a patient's body. To date, there are no available standardized methods for monitoring *in vivo* behaviors and targeting efficacy of injected CAR T-cells. The most common (but limited) techniques used to identify CAR T-cells in the body are flow cytometry, biopsy/immunohistochemistry (IHC), enzyme-linked immunosorbent (ELISpot) or polymerase chain reaction (PCR) [9-12]. Unfortunately, none of these techniques can monitor CAR T-cells within a live body. In order to optimize the efficacy of CAR T-cell immunotherapy and to predict potential toxicities, it is necessary to develop a noninvasive imaging system that can enable monitoring of CAR T-cell trafficking in a real-time manner. Image-based data provides a great deal of information concerning actual tracking, targeting patterns, real-time distributions, and *in vivo* maintenance for CAR T-cell therapies.

Additionally, the FDA Guidance for Industry: Preclinical Assessment of Investigational Cellular and Gene Therapy Products (updated 11/2013) acknowledged that the fate of investigational cell therapy, after *in vivo* administration, is important for characterizing the product's activity and safety profile. To determine distribution after cell administration, imaging methods such as radioisotope-labeled cells, genetically modified cells (e.g., green fluorescent protein expression), and

nanoparticle-labeled cells (e.g., iron-dextran nanoparticles) are recommended. Unlike conventional drugs, cell therapies must acquire data through *in vitro* experiments to determine pharmacological activities or unrecognized toxicity. Therefore, animal models are generally recommended for evaluating cell therapies because basic information on the initial behavior, organ distribution, and targeting in the body after cell therapy are all important. Nuclear medical imaging is a proper method that enables real-time monitoring of cells in the body.

Positron emission tomography (PET) is a diagnostic imaging method that can evaluate metabolic activities in the body by injecting a radioactive tracer as a nuclear medicine functional imaging technique. PET is a unique and important tool for tracking cells in preclinical and clinical studies [13, 14]. It can be used for translational research, moving from preclinical to clinical studies, because the technology features high sensitivity and spatial resolution. There are two ways to image cells: direct and indirect labeling. This study was designed to monitor CAR T-cells via direct labeling. Direct labeling of cells immediately marks the cells with a radioisotope through covalent bond conjugation. Cell migration and distribution immediately after cell injection can be monitored. In this study, the method of direct labeling for CAR T-cells was established. Especially since CAR T-cells can be manipulated *ex vivo*, it is possible to track the behavior and the distribution of small numbers of radiolabeled cells after *in vitro* labeling.

^{89}Zr has a long physical half-life (78.4 hours) and is therefore suitable for tracking the behavior of CAR T-cells in the body. In previous reports, cells were directly labeled using isotopes conjugated with ^{89}Zr-oxine or desferrioxamine (DFO) moiety for cell imaging [15-18]. Recently, Weist et al. proposed that ^{89}Zr-oxine would be a clinically-translatable platform for real-time assessment of cell therapies, especially CAR T-cells [19]. However, Bansal et al. [16] reported that the ^{89}Zr-DFO labeling strategy was superior to ^{89}Zr-oxine, with increased cell stability and viability. Based on existing preclinical applications, the aim of this study was to assess the feasibility of real-time trafficking of ^{89}Zr-DFO-labeled CAR T-cells using PET imaging.

Materials and Methods

Study design and ethics statement

The research protocol of this preclinical experimental study with animals was approved by the Institutional Animal Care and Use Committee of the Asan Institute for Life Science (registration no. 2017-12-085). Mice were maintained in accordance with the Institutional Animal Care and Use Committee guidelines of the Asan Institute for Life Science.

The study scheme is shown in Figure 1. After preparation of CAR-expressing Jurkat (Jurkat/CAR) T-cells and CAR T-cells from human peripheral blood mononuclear cells (hPBMC), all cells were radiolabeled with ^{89}Zr-DFO. The viability, proliferation ability, and function of ^{89}Zr-DFO-labeled cells were evaluated. PET/magnetic resonance (MR) imaging was completed after injection of ^{89}Zr-DFO-labeled Jurkat/CAR T-cells or CART-cells into mice with a xenograft for cell trafficking. The imaging data were compared with *ex vivo* experiments performed with unlabeled Jurkat/CAR T-cells.

Synthesis of the ^{89}Zr-DFO complex for cell labeling

$^{89}ZrCl_4$ was prepared from ^{89}Zr-oxalate (Perkin almer) using QMA cartridge and 1.0 N HCl. 285 μl of HBSS buffer containing 2.8 nmol of DFO and 62.9 ± 29.6 MBq of $^{89}ZrCl_4$ were used to prepare the ^{89}Zr-DFO complex. After checking the pH of the reaction mixture, 11.6 ± 2.2 μl of 1 N NaOH was added to adjust the pH for cell labeling. The reaction mixture was incubated in a thermomixer at 37℃ and 550 rpm overnight until labeling efficiency reach >95%. Radiolabeling efficiency was determined by radio thin-layer chromatography (radioTLC) using iTLC SG with 50 mM DTPA as developing solution.

Labeling of CAR T-cells with ^{89}Zr-DFO

CD19-targeting Jurkat/CAR T-cells were produced as previously described [20] and provided by Dr. Sang-Jin Lee of the National Cancer Center. The construction map and CD19 expression level are shown on Fig 2A and B, respectively. Cell labeling with ^{89}Zr-DFO was performed with a slight modification of the previously described method [15]. Briefly, the Jurkat/CAR T-cells were counted, harvested and washed once with HBSS buffer (pH 7.5). Then, 185 kBq/100 μl HBSS buffer of ^{89}Zr-DFO was added to each glass tube with 5×10^6 cells in 500 ml HBSS buffer and incubated in a thermomixer at 37 ℃ for 30 minutes (Eppendorf, Germany) with gentle shaking. After incubation, 1 ml of cold HBSS buffer was added and the

solution was centrifuged with 1200 rpm for 5 minutes at 4°C in order to separate the supernatant. The supernatant was collected in a new tube and this washing process was repeated three times. The final cell labeling efficiency was calculated as follows: Labeling efficiency (%) = [cell activity (cpm)/{cell activity (cpm) + supernatant activity (cpm)}] × 100. CAR T-cells from hPBMC were labeled with the same procedure as the CAR Jurkat T-cells, but ^{89}Zr-DFO 74 kBq/100 μl HBSS buffer was added to each tube.

Cell viability and proliferative activity of ^{89}Zr-DFO labeled cells

To investigate the cell viability and proliferation rates, ^{89}Zr-DFO-labeled and unlabeled cells were seeded to $2 \times 10^4 \sim 5 \times 10^5$ cells/well in 6 well plates containing 5 ml of culture medium. After seeding, the cell viability was assessed using trypan blue exclusion assay at 1 hour, 1 day, 3 days and 7 days. At the same time, the cell proliferation rate was compared with unlabeled cells. The seeded cells were maintained at 37 °C, 5% CO_2 incubator. Unlabeled cells served as controls.

Function test for ^{89}Zr-DFO labeled cells

To determine the function of ^{89}Zr-DFO-labeled Jurkat/CAR T-cells, the target cell-specific cytokine IL-2 production ability was evaluated with Raji (CD19 positive cells) and K562 (CD19 negative cells) cancer cell lines as target cells, and compared with the results obtained from unlabeled Jurkat/CAR T-cells. For IL-2 secretion assay, ^{89}Zr-DFO-labeled cells were seeded 4×10^4 cells/well in 6 well plates and were cultured for 12 or 36 hours at a 4:1 ratio [effector cells: target cells (Raji or K562 cells)]. Human IL-2 ELISA assay (RayBiotech, GA, USA) was performed according to the instructions of the manufacturer. To observe the function of ^{89}Zr-DFO-labeled hPBMC CAR T-cells, IFN-γ release assay (RayBiotech, GA, USA) was additionally performed according to the instructions of the manufacturer.

Animal model establishment

To develop a mouse xenograft model, NSG mice (female, 5–6 weeks old, 20–22 g) from Jackson Laboratory (USA) were used. To compare tumor targeting of CAR T-cells, 5×10^6 of Raji (Burkitt lymphoma, ATCC, CCL-86) cells were injected into the left flank and 5×10^5 of K562 (chronic myelogenous leukemia, ATCC, CCL-243) cells were injected into the right flank of each mouse, at the same time. Over the following 5–7 days, the tumors reached a volume of 50 to 100 mm^3. Tumor volume was measured 3 times per week and calculated as length × width × height × π/6 (mm^3).

Animal PET-MR imaging and image analysis

PET-MR fusion imaging was performed using nanoScanPET/MRI system (1T, Mediso, Hungary). ^{89}Zr-DFO-labeled Jurkat/CAR T-cells (n, median: 4.1 × 10^6, range: 3.1–5.4×10^6; radioactivity, median: 907 kBq, range: 481–1221 kBq) were slowly injected intravenously through a tail vein using a 26 G syringe. Before PET image acquisition, the mice were kept under anesthesia (1.5% isoflurane in 100% O_2 gas). Imaging was performed on days 0 (median: 106 minutes, range: 92–132 minutes, after the injection), 1, 2, 5, 6 and 7. The T1 weighted with gradient-echo 3D sequence (TR = 25 ms, TEeff = 3.4, FOV = 64 mm, matrix = 128 × 128) MR images were acquired, followed by static PET images for 10 minutes (days 0 and 1), 20 minutes (day 2), or 30 minutes (days 5, 6 and 7) in a 1–5 coincident in a single field of view with the MR imaging range. Body temperature was maintained with heated air on the animal bedding (Multicell, Mediso, Hungry) and a pressure-sensitive pad was used for respiratory triggering. PET images were reconstructed using Tera-Tomo 3D, in full detector mode, with all the corrections on, high regularization, and 8 iterations. A three-dimensional volume of interest (VOI) was applied to organs (brain, left ventricle of heart, lung, liver, kidney, spleen, and bone) and tumors on the reconstructed PET and MR images using the InterView Fusion software package (Mediso, Hungary) and quantitative analysis procedures. The VOI sites were analyzed using the following formula: %ID = radioactivity in each organ divided by injected radioactivity.

***Ex vivo* bio-distribution study**

Immediately after the PET-MR image acquisition on day 7, all mice were sacrificed. Their organs (brain, heart, lung, liver, spleen, kidney, stomach, intestine, bone, muscle, etc.) and tumors were excised, weighed, and counted in a gamma-counter for 5 minutes. The % injected dose (ID) values were obtained after normalization to the weight of each organ.

Flow cytometry analysis

To validate the biodistribution of Jurkat/CAR T-cells after injection, *ex vivo* immunostaining of organs was performed. The mouse organs (liver, spleen) were harvested on day 3 after injection of unlabeled Jurkat/CAR T-cells (2 × 10^7/200 μl) into the NSG mice with tumors via their tail veins (n = 2). Tissues were ground using a gentleMACS™ dissociator (Miltenyi Biotec, Germany) according to the supplier's protocol. A mouse cell depletion kit (Miltenyi Biotec, Germany) was used

to separate the Jurkat/CAR T-cells from mouse cells. After counting the live cells, the human T-cell isolation kit (Miltenyi Biotec, Germany) was used according to the supplier's protocol. Red blood cells were removed using a RBC lysing buffer (Sigma Aldrich, MO) for 1 minute, followed by washing and re-suspension in 1 × HBSS containing 1% FBS. The separated cells were used with PE-conjugated anti-CD3. The analysis staining process was the same as that used *in vitro*. Data were acquired from the stained cells using BD FACS CantoII flow cytometry (BD Biosciences), and the results were analyzed with FlowJo software (Treestar Inc., Ashland, OR).

Preparation of genomic DNA and Alu PCR analysis

To validate the biodistribution of Jurkat/CAR T-cells after injection, PCR analysis of *ex vivo* tissue (n = 3) was also performed. At 3 days after injection of 2×10^7 of Jurkat/CAR T-cells into the mice through the tail veins, the mice were sacrificed and brain, heart, lung, liver, spleen, and kidney samples were collected. For Alu PCR assay to detect injected human cells, genomic DNA was extracted from tissue samples using the QIAamp®IAamp (the QIAampQiagen, Germany) according to the protocol of the manufacturer. The primers used in this study were as follows: for human Alu, 5'- CACCTGTAATCCCAGCACTTT-3' (forward primer) and 5'-CCCAGGCTGGAGTGCAGT-3' (reverse primer). Real-time PCR was performed by SYBRercturerRealtime PCR Master Mix (TOYOBO, Japan) and the ABI 7500 Fast Real-time PCR system (Applied Biosystems, CA, USA) according to the manufacturers' instructions. The PCR experimental conditions were 95 ℃ for 10 minutes, followed by 40 cycles at 95 °C for 15 seconds and 60 °C for 1 minute. This was followed by melting curve cycles at 95 °C for 15 seconds, at 60 °C for 1 minute, and finally at 95 °C for 15 seconds. Concentrations that 1, 5, and 25 dilution based on 10^6 cells of CAR Jurkat T-cells expressing CD19 were used as a standard. The results indicated the amount of Alu expression, based on the standard.

Immunohistochemistry analysis

IHC analysis was performed as described previously [21]. The mice were sacrificed on day 3 (n = 3) or day 7 (n = 2) after Jurkat/CAR or hPBMC CAR T-cells were injected into tumor-bearing mice. For the day 3 group, after injection of Jurkat/CAR T-cells, the liver, spleen, and tumors were harvested and fixed within paraffin blocks for IHC staining. The slides were stained with an anti-CD3 antibody (Abcam, UK) with the Dako REAL™ EnVision™ Detection System (Agilent Technologies, Inc., CA, USA) and were counter-stained with hematoxylin.

Statistical analysis

Data are expressed as means ± SDs unless otherwise specified. A value of $p < 0.05$ was considered statistically significant. The Kruskal-Wallis test was used to determine differences between time points after ^{89}Zr-DFO labeling. Statistical analyzes were performed using GraphPad Prism (GraphPad Software, CA, USA).

Results

Labeling efficiency, viability and proliferative ability of ^{89}Zr-DFO-labeled Jurkat/CAR T-cells and CAR T-cells

The ^{89}Zr-DFO labeling efficiency of Jurkat/CAR T-cells was 72.8% ± 11.0% at 185 kBq (Figure 3A). Cell viability after ^{89}Zr-DFO labeling was 95.2% ± 1.2%, similar to levels obtained before labeling. The concentration of radioactivity for Jurkat/CAR T-cells was 103.6 kBq/10^6 cells. The labeling of hPBMC CAR T-cells proceeded to 74 kBq. ^{89}Zr-DFO labeling efficiency was similar to Jurkat/CAR T-cells (Figure 3A). The ^{89}Zr-DFO-labeled hPBMC CAR T-cells showed a radioactivity concentration of 98.1 kBq/10^6 cells.

The cell viability and cell proliferative ability were checked at 1 hour, day 1, day 3, and day 7 after ^{89}Zr-DFO cell labeling. There was no statistically significant difference in cell viability, although viability decreased over time after cell labeling (p = 0.24, 1 hour: 92.6 % ± 3.1%, day 1: 89.4 % ± 4.4%, day 3: 85.7 % ± 8.1%, day 7: 89.0 % ± 4.9%, respectively) (Figure 3B). However, the ^{89}Zr-DFO-labeled cells showed decreased proliferative ability in a time-dependent manner (Figure 3C). At 1 hour after cell labeling, cell proliferation ability was not significantly changed, compared with unlabeled cells (p = 0.25). However, cell proliferation significantly decreased over time (1 hour: 1.28 ± 0.44, day 1: 0.69 ± 0.13, day 3: 0.54 ± 0.15, and day 7: 0.49 ± 0.32, respectively).

Functional test for ^{89}Zr-DFO labeled Jurkat /CAR T-cells or CAR T-cells

CAR T-cell function was assessed by target cell-specific cytokine IL-2 production ability at 12 and 36 hours after cell labeling. Both ^{89}Zr-DFO-labeled and unlabeled Jurkat/CAR T-cells induced IL-2 release in the positive target cells (Raji) at similar levels (74.1 vs 76.5 ng/ml at 12 hours, 86.4 vs 87.1 ng/ml at 36 hours) (Figure 4A). IL-2 was not released in negative target cells (K562) which did not react with Jurkat/CAR T-cells.

The IL-2 secretion of hPBMC ^{89}Zr-DFO-labeled CAR T-cells was also similar to that observed in unlabeled cells (Figure 4B). When hPBMC CAR T-cells were added to Raji cells expressing the targeted CD19 cells, the secretion of IFN-γ involved in cell cytotoxicity was maintained after ^{89}Zr-DFO labeling (69.3 vs 71.6 ng/ml) (Figure 4C).

Trafficking of ^{89}Zr-DFO labeled Jurkat/CAR T-cells with PET/MR imaging

After injection of ^{89}Zr-DFO-labeled Jurkat/CAR T-cells through the tail veins of

the mice, PET/MR imaging was used for noninvasive real-time tracking of injected cells *in vivo*. The Jurkat/CAR T-cells were initially located in the lungs, then redistributed to the liver and spleen (Figure 5A). In more detail, the injected ^{89}Zr-DFO-labeled Jurkat/CAR T-cells were found mainly in the lung (25.0% ± 3.7%ID) and liver (23.4% ± 5.3%ID) during the first 1 hour (Figure 5B). Over time, the CAR T-cells gradually migrated from the lungs and accumulated in the liver. On the final image taken on day 7, most cell signals had migrated from the lung (3.9% ± 0.6%ID) to the liver (35.7% ± 1.0%ID). However, radioactivity accumulation was not evident in either CD19-positive Raji or CD19-negative K562 tumors. Immediately after PET/MR imaging on day 7, the mice were sacrificed, then their organs and tumors were isolated to measure the radioactivity of injected cells *ex vivo*. Biodistribution data measured *ex vivo* on day 7 showed similar patterns of distribution assessed by PET images as shown in Figure 5C and Table 1.

PET/MR imaging with^{89}Zr-DFO-labeled CAR-T-cells from hPBMC also showed similar biodistribution of cells after tail vein injection. Increased radioactivity in the tumors was not observed, which would have suggested CAR T-cell homing (Figure 6). Compared to the whole-body activity on PET imaging on the day of injection, decay-corrected total activity remained similar on serial images from days 1, 2, 5, 6, and 7 (95.7% ± 0.9%, 96.8% ± 2.5%, 103.6% ± 4.4%, 108.8% ± 7.5%, 105.1% ± 5.7%, respectively).

Flow cytometry, Alu PCR and immunohistochemistry for *ex vivo* organ study

Biodistribution was compared after injection of unlabeled Jurkat/CAR T-cells using both imaging and non-imaging methods. For flow cytometry, the liver and spleen tissue samples from mice were separated into single cells. After the initial separation an average number of 3.05×10^7 and 1.67×10^6 cells per mouse were harvested. After depletion of mouse liver cells, an average of 4.74×10^4 cells were obtained after using a human T-cell isolation kit. In contrast to the negative control stained with isoform antibody, CD3 expressing CAR T-cells were distributed in 95.7% of the spleen and 60.3% of the liver (Figure 7A).

Organ distributions of Jurkat/CAR T-cells were confirmed through Alu PCR. The blood, heart, lung, liver, spleen and kidney were sampled, and CD19 CAR T-cells were distributed in all 6 organs. The relative Alu expression was determined by measuring blood, and the fold was as follows: brain (15.1 ± 5.8), heart (6.2 ± 7.2), lung (38.5 ± 34.8), liver (212.2 ± 225.4), spleen (70.3 ± 9.4), kidney (9.4 ± 6.4) and gut (17.5 ± 8.9) (Figure 7B).

Immunohistochemical staining with CD3 of liver and spleen tissues confirmed the presence of Jurkat/CAR T-cells in the liver and spleen, in contrast to control tissue from mice not injected with Jurkat/CAR T-cells (Figure 8A & B). Immunohistochemical staining of Raji and K562 tumors of the day 3 group with CD3 showed barely-visible stained cells in the periphery of the tumors (Figure 8C). In the day 7 group, hPBMC CAR T-cells showed proliferation throughout Raji tumors; however, Jurkat/CAR T-cells were not visualized (Figure 8D). No K562 tumors were stained with CD3 antibody.

Discussion

In this study, CAR T-cells could be tracked *in vivo* for 7 days after intravenous injection by ^{89}Zr-DFO labeling and PET/MR images. CAR T-cells initially reached the lungs and gradually migrated to the liver and spleen by day 1, where they remained for the rest of the experimental period. The organ distribution of ^{89}Zr-DFO-labeled cells quantitatively assessed by PET/MR images was confirmed with an *ex vivo* biodistribution study where the radioactivity was analyzed of each organ harvested from the mice on day 7. This pattern of distribution was observed in both ^{89}Zr-DFO labeling of Jurkat/CAR T-cells and CAR T-cells from human peripheral blood. The distribution of cells after injection of unlabeled Jurkat/CAR T-cells was also confirmed by flow cytometry, Alu PCR, and IHC with isolated tissues from sacrificed mice on day 3. The distribution after cell administration could be reliably and noninvasively tracked using ^{89}Zr-DFO labeling of CAR T-cells and PET/MR imaging, as suggested by FDA guidance. In quantitative analysis of organ distribution of cell populations, previous studies with radioisotope labeling had a lack of specific organ distribution data because of the difficulties in gathering anatomical information with PET alone. The current study was performed using a hybrid imaging system. Here PET and MR allowed organ-specific detection of the cell signal, along with structural information. The quantitative nature of PET allows for longitudinal studies that provide information on relative levels of CAR T-cells at both the site of disease and potential off-target sites of accumulation. Monitoring the locations and potential secondary sites involved in CAR T-cell trafficking enables us to characterize the activity of administered cells and safety profile.

^{89}Zr-DFO was used for labeling CAR T-cells in this study, instead of ^{89}Zr-oxine complex, which was used by Weist et al. [19], because it has more stable covalent binding between DFO and cell surface protein [16]. With ^{89}Zr-DFO labeling of human immune cells, radioactivity concentrations of labeled cells of up to 0.5 MBq/10^6 cells were achieved without a negative effect on cellular viability and cell efflux studies showed high radiolabel stability, with virtually no loss of tracer for up to 7 days [16]. Whereas a significant amount of ^{89}Zr-oxine can efflux from various kind of cells, and there is potential uptake of small amount of free ^{89}Zr released from cells into the bones or kidneys, as shown in the report by Weist et al. [19]. In our PET images of ^{89}Zr-DFO-labeled cells, less radioactivity accumulated in the bones and kidneys until 7 days after injection, compared with the results reported with ^{89}Zr-oxine labeled cells. Furthermore, the measured total activity on the initial PET images was maintained on serial PET images with decay correction (102.0% ±

6.7%) without significant loss of activity from the body. These findings suggest stable cell labeling by ^{89}Zr-DFO *in vivo*, as demonstrated in other studies.

The cell viability and functionality, such as cytokine production, were not affected by labeling CAR T-cells with ^{89}Zr-DFO, at radioactivity cell concentration of 98 kBq/10^6 cells. However, proliferation ability was slightly decreased over the next several days compared with unlabeled cells. It is important to consider the effect of radiation dose on cells of hematopoietic origin, which tend to be radiation-sensitive. Especially, ^{89}Zr has high-energy gamma emissions of 908.97 keV, which may limit the radioactive dose; further, the radiolabeling procedure is potentially cytotoxic. Therefore, the dose of ^{89}Zr-DFO was reduced when labeling CAR T-cells from hPBMC to 74 kBq/10^6 cells, compared with 185 kBq/10^6 cells in the labeling of Jurkat/CAR after careful dose optimization because of hPBMC sensitivity.

The distribution pattern of CAR T-cells in this study was similar with previous studies. Following intravenous administration, human T-cells migrated in a manner similar to that reported in humans, but penetrated poorly into established tumors. Following intravenous administration, human T-cells initially reached the lungs where they remained for more than 4 hours. Thereafter, the T-cells redistributed to the liver, spleen, and lymph nodes [21]. This pattern was observed using all T-cell populations tested, irrespective of transgene cargo or tumor status, and closely mimicked patterns of migration seen in human (via infusion) [22-24] or murine T-cell [25, 26] recipients. According to Charoenphun et al., ^{89}Zr-oxine labeled myeloma cells were injected intravenously and were found within the lungs at 30 minutes after injection, but migrated to the liver and spleen on day 1. This distribution continued until day 7 [27]. Similar distributions of ^{89}Zr-oxine labeled dendritic cells were observed by Sato et al. [18]. Weist et al. also found that the highest CAR T-cell activity in the spleen, followed by the liver [19]. In these studies, lung activity was significantly lower on day 7 than activity in the liver or spleen. In contrast, Bansal et al. found that mesenchymal stem cells exhibited persistently high activity in lung images, up to day 7, and their biodistribution study also showed the highest activity in the lung (approximately 50%ID), followed by the liver (approximately 25%ID) [16]. It has been suggested that slow migration of transferred T-cells through the lungs may be due to low pulmonary circulatory pressure, coupled with the narrowing of capillaries during expiration [24]. Importantly, activated T-cells cross the pulmonary circulation with a reduced intravascular velocity, compared to their inactivated or naive counterparts [28, 29]. This delay may reflect an enhanced interaction between high-affinity state LFA-1 (T-cells) and ICAM-1 (endothelium), in part [28]. Delayed clearance of highly

activated T-cells during their first pass through the lungs may be highly relevant to the development of pulmonary toxicity that can occur following infusion of CAR T-cells. In one such published incident, rapid onset of fatal adult respiratory distress syndrome occurred following infusion of $>10^{10}$ T-cells, targeted against ErbB2 using a trastuzumab scFv coupled to a fused CD28/4-1BB/CD3ζ endoplasmic domain [30].

In this study, T-cell migration to the target tumor was not observed on PET images, unlike reports by Sato et al. and Weist et al. It was disappointing to observe that only a minority of intravenously administered CAR T-cells migrated to tumor deposits, even though CD19 CAR T-cells were used with proven efficacy in animals and humans. There are several potential causes of this phenomenon. Jurkat/CAR T-cells were used in this study because CAR T from hPBMC are leukemia cells, and not true T-cells. Although Jurkat cells were used for convenience in this experiment, their actual biologic behavior may be different from normal T-cells. Second, the solid subcutaneous tumor xenograft model used in this study was a different tumor environment from that of human acute lymphocytic leukemia of the blood, for which CD19-CAR T-cells have shown a dramatic therapeutic effect. Also, the differences in the antigen-presenting status of the tumor, tumor microenvironment etc. between the xenograft model generated from Raji cells, and those of previous studies by Sato et al. (B16 murine melanoma cells [18]) and Weist et al. (prostate cancer PC3-overexpressed cells [19]) may have affected the accumulation of CAR T-cells within tumor tissue [31]. Third, detection of cell trafficking by imaging carries important limitations. Cell trafficking may not be detectable via PET imaging when small amounts of T-cells, below detectable limits, are injected. Furthermore, after homing to the tumor, activated CAR T-cells can proliferate and dilute the labeling signal. In our IHC & PET imaging data, hPBMC CAR T-cells showed proliferation within Raji tumor tissues after CD19 targeting (Figure 8D); however, there are rare PET imaging signals in tumors.

There are several limitations to this study. First, therapeutic effect of CAR T-cells was not shown in this study, because the experiments were conducted mainly with Jurkat/CAR T-cells instead of hPBMC CAR T-cells. Limited imaging experiments were possible with hPBMC CAR T-cells and only two mice. Second, the biodistribution study was only performed using direct cell labeling strategies. Direct cell labeling enables observation of the initial behavior of the injected cells and the distribution to the whole-body in real-time with very low background activities. This is, in principle, not present in other host tissues or cells. Direct labeling does not involve genetic manipulation of the therapeutic cells. However, the direct labeling method cannot visualize cell proliferation [32]. The disadvantage of direct cell

labeling is the release of the label from dying cells and the dilution of the label as cells divide, which might impair their detectability. As no new labels can be added to the cells after administration, the tracking imaging time window is maximized after only a few label half-lives are used. With ^{89}Zr-DFO direct cell labeling in this study, the activated proliferative effector cells cannot be monitored after homing to the target tumor. Therefore, further studies that use both direct and indirect labeling strategies, where reporter genes are inserted in the vector, should be carried out with hPBMC CAR T-cells.

Conclusion

With ^{89}Zr-DFO labeling of CAR T-cell, real-time *in vivo* cell trafficking was feasible through PET imaging after administration of cells to the body. Thus, ^{89}Zr-DFO-labeled CAR T-cell PET imaging can be used to investigate cell kinetics, *in vivo* cell biodistribution, and the safety profile of CAR T-cell therapies that are developed.

References

1. Brown CE, Alizadeh D, Starr R, Weng L, Wagner JR, Naranjo A, et al. Regression of Glioblastoma after Chimeric Antigen Receptor T-Cell Therapy. N Engl J Med. 2016;375:2561-9.
2. Curran KJ, Pegram HJ, Brentjens RJ. Chimeric antigen receptors for T cell immunotherapy: current understanding and future directions. J Gene Med. 2012;14:405-15.
3. Ho WY, Blattman JN, Dossett ML, Yee C, Greenberg PD. Adoptive immunotherapy: engineering T cell responses as biologic weapons for tumor mass destruction. Cancer Cell. 2003;3:431-7.
4. Sadelain M, Riviere I, Brentjens R. Targeting tumours with genetically enhanced T lymphocytes. Nat Rev Cancer. 2003;3:35-45.
5. Kershaw MH, Westwood JA, Darcy PK. Gene-engineered T cells for cancer therapy. Nat Rev Cancer. 2013;13:525-41.
6. Brentjens RJ, Davila ML, Riviere I, Park J, Wang X, Cowell LG, et al. CD19-targeted T cells rapidly induce molecular remissions in adults with chemotherapy-refractory acute lymphoblastic leukemia. Sci Transl Med. 2013;5:177ra38.
7. Grupp SA, Kalos M, Barrett D, Aplenc R, Porter DL, Rheingold SR, et al. Chimeric antigen receptor-modified T cells for acute lymphoid leukemia. N Engl J Med. 2013;368:1509-18.
8. Kalos M, Levine BL, Porter DL, Katz S, Grupp SA, Bagg A, et al. T cells with chimeric antigen receptors have potent antitumor effects and can establish memory in patients with advanced leukemia. Sci Transl Med. 2011;3:95ra73.
9. De Oliveira SN, Wang J, Ryan C, Morrison SL, Kohn DB, Hollis RP. A CD19/Fc fusion protein for detection of anti-CD19 chimeric antigen receptors. J Transl Med. 2013;11:23.
10. Teachey DT, Lacey SF, Shaw PA, Melenhorst JJ, Maude SL, Frey N, et al. Identification of Predictive Biomarkers for Cytokine Release Syndrome after Chimeric Antigen Receptor T-cell Therapy for Acute Lymphoblastic Leukemia. Cancer Discov. 2016;6:664-79.
11. Wang H, Du X, Chen WH, Lou J, Xiao HL, Pan YM, et al. Establishment of a Quantitative Polymerase Chain Reaction Assay for Monitoring Chimeric Antigen Receptor T Cells in Peripheral Blood. Transplant Proc. 2018;50:104-9.
12. Zheng Z, Chinnasamy N, Morgan RA. Protein L: a novel reagent for the detection of chimeric antigen receptor (CAR) expression by flow cytometry. J

Transl Med. 2012;10:29.
13. Adonai N, Adonai N, Nguyen KN, Walsh J, Iyer M, Toyokuni T, et al. Ex vivo cell labeling with 64Cu-pyruvaldehyde-bis(N4-methylthiosemicarbazone) for imaging cell trafficking in mice with positron-emission tomography. Proc Natl Acad Sci U S A. 2002;99:3030-5.
14. Hofmann M, Wollert KC, Meyer GP, Menke A, Arseniev L, Hertenstein B, et al. Monitoring of bone marrow cell homing into the infarcted human myocardium. Circulation. 2005;111:2198-202.
15. Abou DS, Ku T, Smith-Jones PM. In vivo biodistribution and accumulation of 89Zr in mice. Nucl Med Biol. 2011;38:675-81.
16. Bansal A, Pandey MK, Demirhan YE, Nesbitt JJ, Crespo-Diaz RJ, Terzic A, et al. Novel (89)Zr cell labeling approach for PET-based cell trafficking studies. EJNMMI Res. 2015;5:19.
17. Roca M, de Vries EF, Jamar F, Israel O, Signore A. Guidelines for the labelling of leucocytes with (111)In-oxine. Inflammation/Infection Taskgroup of the European Association of Nuclear Medicine. Eur J Nucl Med Mol Imaging. 2010;37:835-41.
18. Sato N, Wu H, Asiedu KO, Szajek LP, Griffiths GL, Choyke PL. (89)Zr-Oxine Complex PET Cell Imaging in Monitoring Cell-based Therapies. Radiology. 2015;275:490-500.
19. Weist MR, Starr R, Aguilar B, Chea J, Miles J, Poku E, et al. Positron emission tomography of adoptively transferred chimeric antigen receptor T cells with Zirconium-89 oxine. J Nucl Med. 2018.
20. Milone MC, Fish JD, Carpenito C, Carroll RG, Binder GK, Teachey D, et al. Chimeric receptors containing CD137 signal transduction domains mediate enhanced survival of T cells and increased antileukemic efficacy in vivo. Mol Ther. 2009;17:1453-64.
21. Parente-Pereira AC, Burnet J, Ellison D, Foster J, Davies DM, van der Stegen S, et al. Trafficking of CAR-engineered human T cells following regional or systemic adoptive transfer in SCID beige mice. J Clin Immunol. 2011;31:710-8.
22. Fisher B, Packard BS, Read EJ, Carrasquillo JA, Carter CS, Topalian SL, et al. Tumor localization of adoptively transferred indium-111 labeled tumor infiltrating lymphocytes in patients with metastatic melanoma. J Clin Oncol. 1989;7:250-61.
23. Pittet MJ, Grimm J, Berger CR, Tamura T, Wojtkiewicz G, Nahrendorf M, et al. In vivo imaging of T cell delivery to tumors after adoptive transfer therapy. Proc Natl Acad Sci U S A. 2007;104:12457-61.
24. Read EJ, Keenan AM, Carter CS, Yolles PS, Davey RJ. In vivo traffic of

indium-111-oxine labeled human lymphocytes collected by automated apheresis. J Nucl Med. 1990;31:999-1006.

25. Smith ME, Ford WL. The recirculating lymphocyte pool of the rat: a systematic description of the migratory behaviour of recirculating lymphocytes. Immunology. 1983;49:83-94.
26. Wagstaff J, Gibson C, Thatcher N, Ford WL, Sharma H, Crowther D. Human lymphocyte traffic assessed by indium-111 oxine labelling: clinical observations. Clin Exp Immunol. 1981;43:443-9.
27. Charoenphun P, Meszaros LK, Chuamsaamarkkee K, Sharif-Paghaleh E, Ballinger JR, Ferris TJ, et al. [(89)Zr]oxinate4 for long-term in vivo cell tracking by positron emission tomography. Eur J Nucl Med Mol Imaging. 2015;42:278-87.
28. Hamann A, Klugewitz K, Austrup F, Jablonski-Westrich D. Activation induces rapid and profound alterations in the trafficking of T cells. Eur J Immunol. 2000;30:3207-18.
29. Looney MR, Thornton EE, Sen D, Lamm WJ, Glenny RW, Krummel MF. Stabilized imaging of immune surveillance in the mouse lung. Nat Methods. 2011;8:91-6.
30. Morgan RA, Yang JC, Kitano M, Dudley ME, Laurencot CM, Rosenberg SA. Case report of a serious adverse event following the administration of T cells transduced with a chimeric antigen receptor recognizing ERBB2. Mol Ther. 2010;18:843-51.
31. Chen Y-P, Zhang Y, Lv J-W, Li Y-Q, Wang Y-Q, He Q-M, et al. Genomic Analysis of Tumor Microenvironment Immune Types across 14 Solid Cancer Types: Immunotherapeutic Implications. Theranostics. 2017;7:3585-94.
32. Kircher MF, Gambhir SS, Grimm J. Noninvasive cell-tracking methods. Nat Rev Clin Oncol. 2011;8:677-88.

Table 1. Quantitative tissue data (%ID/g) of ^{89}Zr-DFO Jurkat/CAR T-cells biodistribution study on day 7 (mean ± SD, n = 4)

Tissues	%ID/g
Raji	0.09 ± 0.01
K562	0.08 ± 0.01
Blood	0.04 ± 0.01
Brain	0.01 ± 0.01
Heart	0.12 ± 0.05
Lung	24.01 ± 8.05
Liver	27.01 ± 2.96
Spleen	118.65 ± 87.60
Kidney	0.30 ± 0.10
Stomach	0.06 ± 0.01
S-intestine	0.04 ± 0.01
L-intestine	0.03 ± 0.01
Ovary	0.26 ± 0.25
T-spine	1.13 ± 0.17
Femur	2.31 ± 1.06
Muscle	0.04 ± 0.01

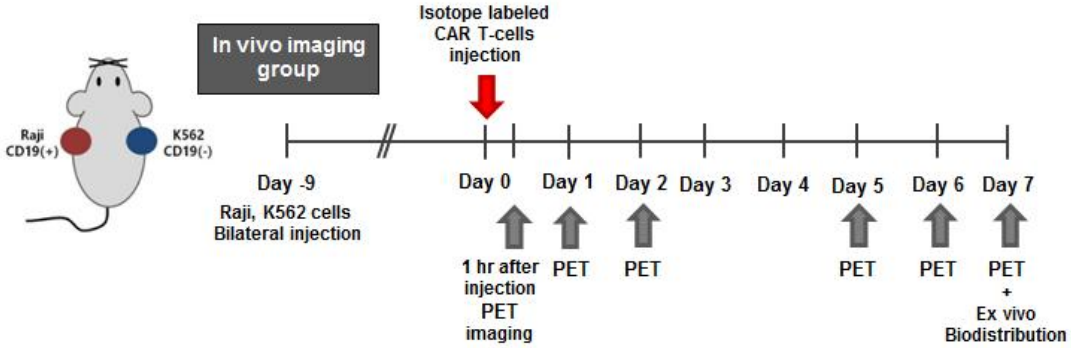

Figure 1. Study scheme

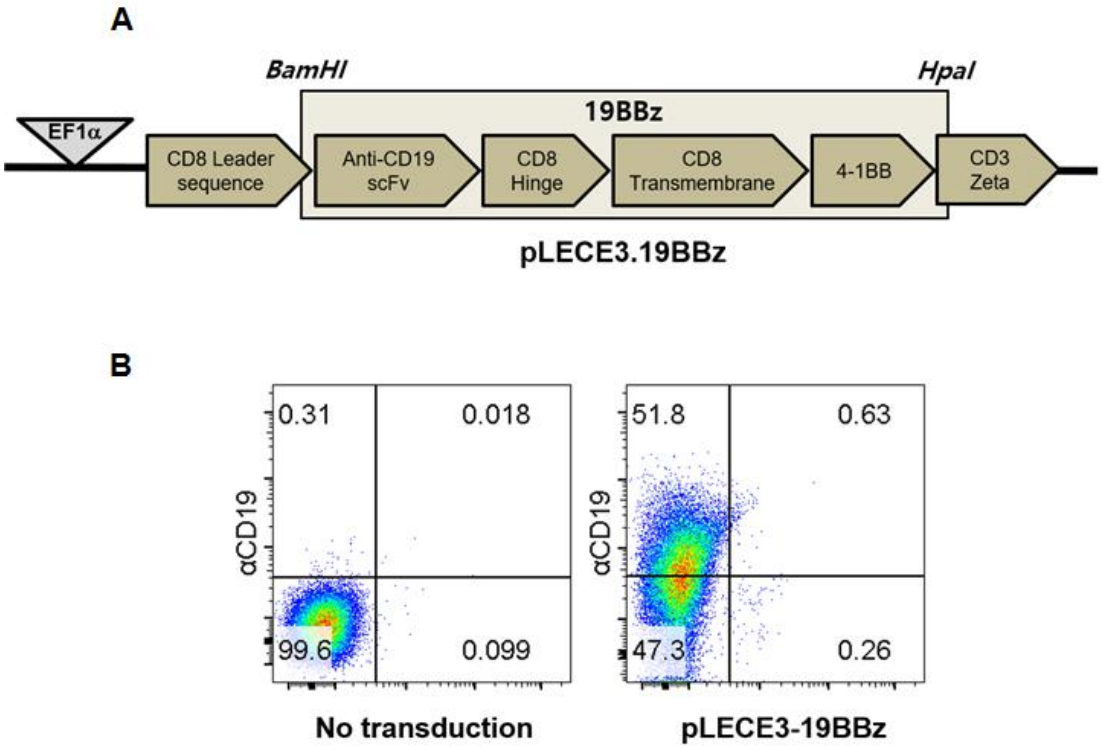

Figure 2. Construction of Jurkat/CAR T-cells specific to CD19.

A. DNA map of pLECE3-19BBz lentivirus vector. B. CAR expression on Jurkat T-cells. Jurkat T-cells were either left alone (left) or transduced with pLECE-19BBz lentiviruses (right).

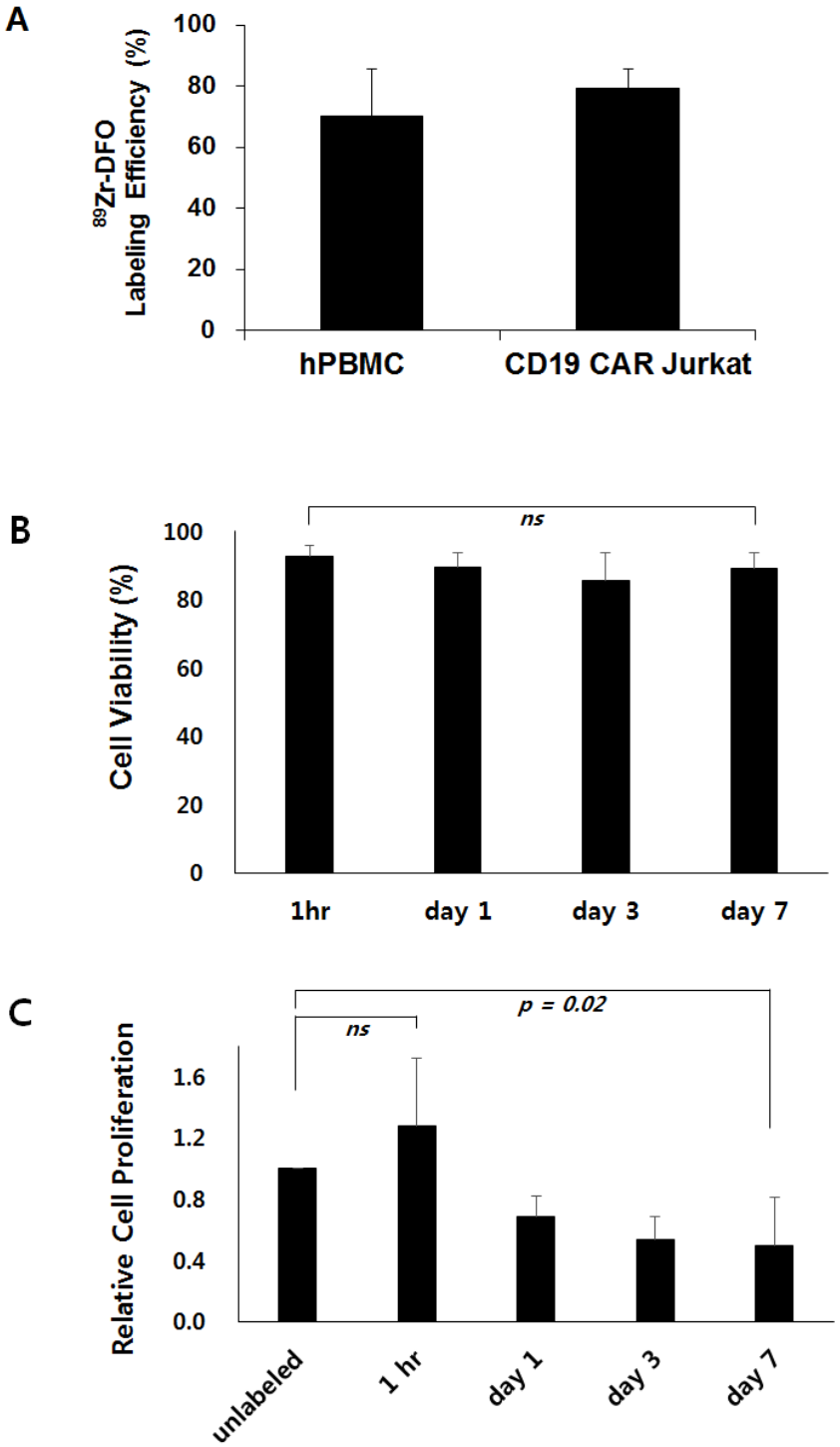

Figure 3. ^{89}Zr-DFO CAR T-cells labeling efficiency, cell viability and relative cell proliferation. A. hPBMC CAR T-cells labeling efficiency after ^{89}Zr-DFO-labeled. B. The cell viability after cell labeling was measured up to 7 days. C. Relative cell proliferation of the labeled CAR T-cells was compared to that not labeled. Data are representative at least three independent experiments. All data are expressed as means and standard deviations.

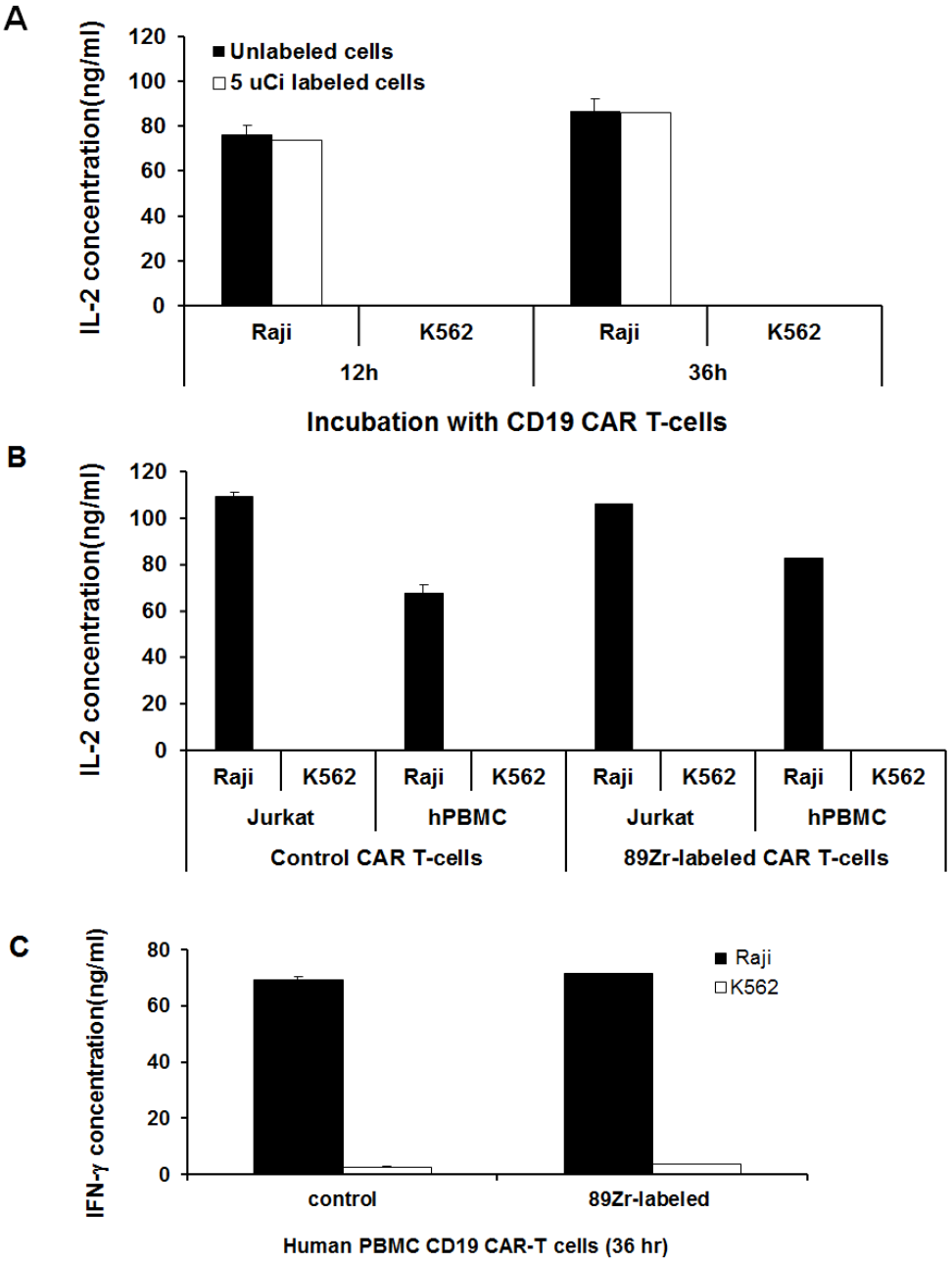

Figure 4. Cell function test after ^{89}Zr-DFO-labeled Jurkat/CAR T-cells and hPBMC CAR T-cells. A. Function test by IL-2 production of ^{89}Zr-DFO-labeled Jurkat/CAR T-cells after incubation with Raji (CD19 positive) or K562 (CD19 negative) cells. Incubation time was for 12 hours or 36 hours and unlabeled cells were used in the experiment as a control group. B. Function test by IL-2 production of ^{89}Zr-DFO-labeled Jurkat/CAR T-cells or hPBMC CAR T-cells after incubation with Raji or K562 cells. C. IFN-γ test of ^{89}Zr-DFO-labeled hPBMC CAR T-cells with Raji or K562 cells. Data are representative at least three independent experiments. All data expressed as means and standard deviations.

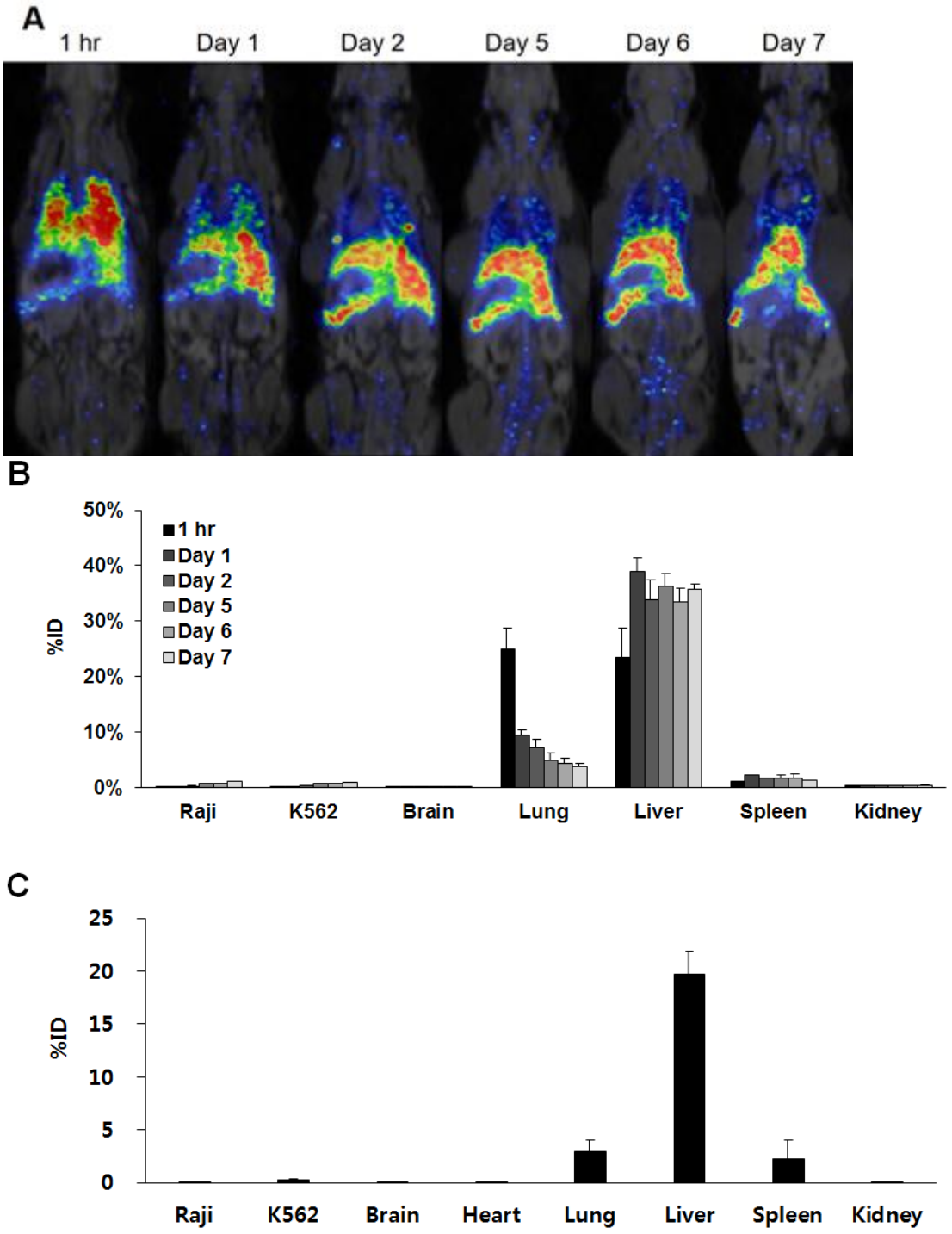

Figure 5. ^{89}Zr-DFO-labeled Jurkat/CAR cells animal PET imaging and analysis.

A. PET images of the whole-body distribution of intravenously-injected ^{89}Zr-DFO-labeled CAR T-cells in NSG mouse xenograft following until day 7. B. %ID values of ^{89}Zr-DFO PET imaging over the following 7 days in representative organs. C. The biodistribution data in *ex vivo* organ measured by model sacrifice after acquisition of the last PET imaging.

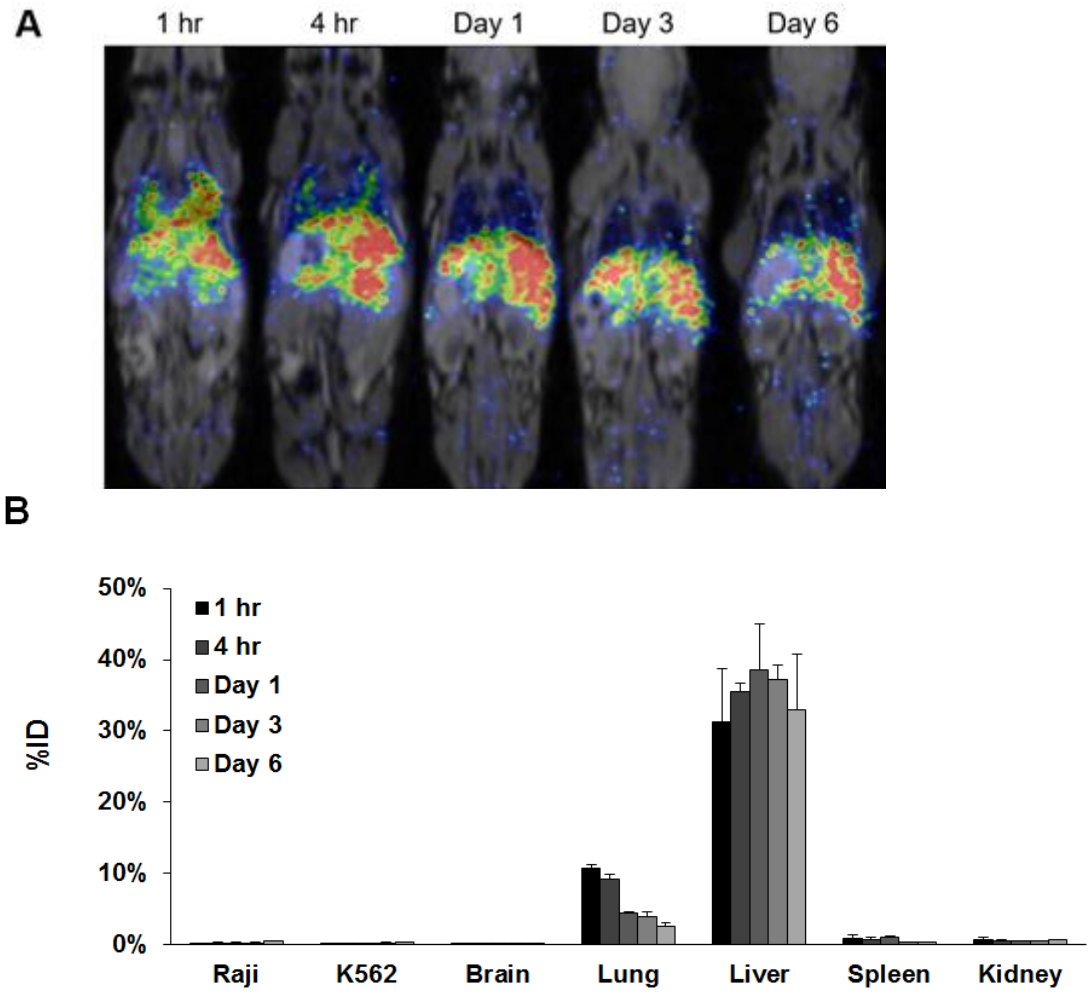

Figure 6. ^{89}Zr-DFO-labeled hPBMC CAR T-cells animal PET imaging and analysis. A. PET images of whole-body distribution for intravenously-injected ^{89}Zr-DFO-labeled hPBMC CAR T-cells in NSG mouse xenograft following until day 6. B. %ID values of ^{89}Zr-DFO PET imaging during 6 days in representative organs. (n = 2)

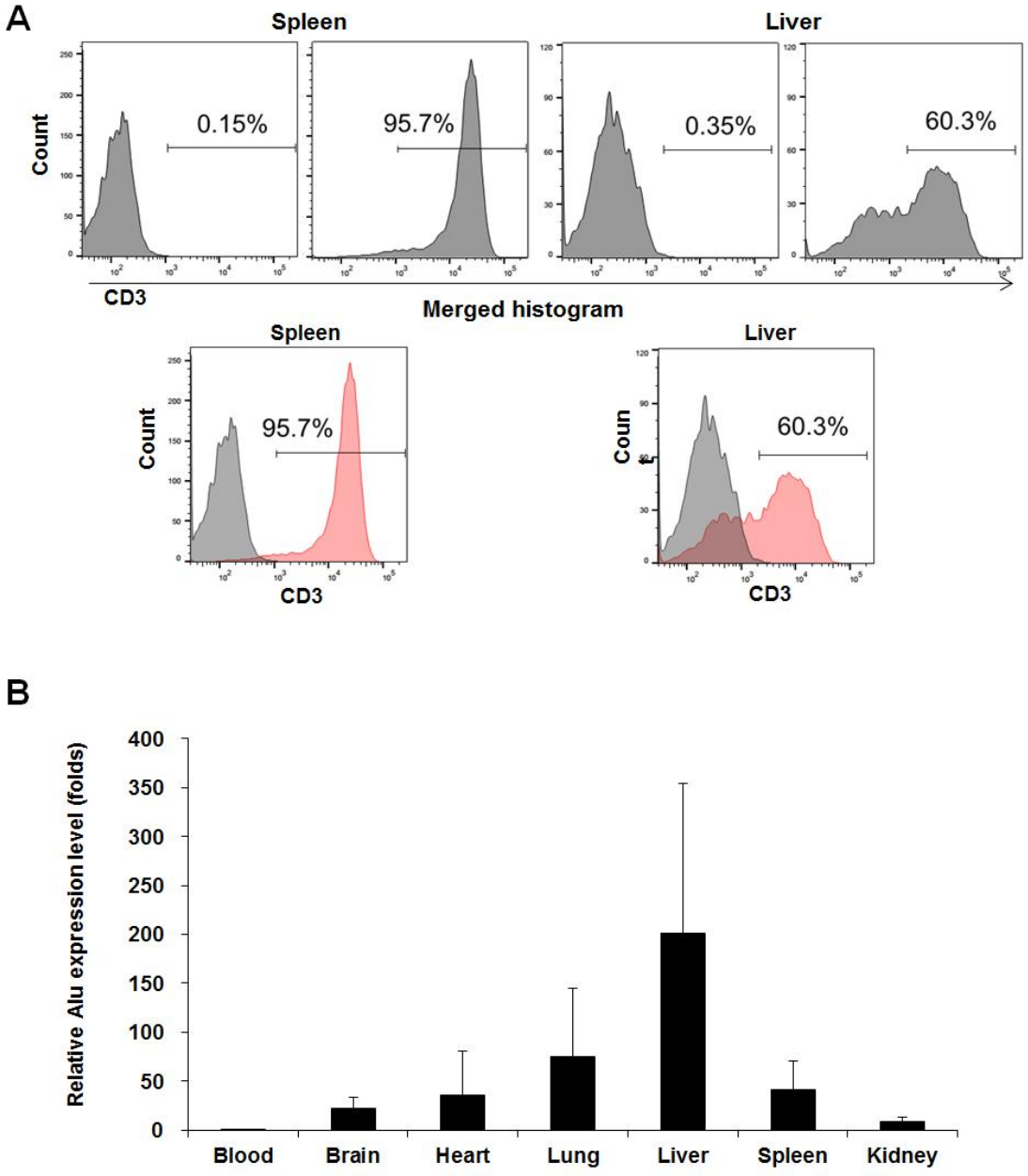

Figure 7. FACS staining and Alu PCR in mouse organs.

A. After sacrificing the mice on day 3 after Jurkat/CAR T-cells injection, graphs of FACS staining for liver and spleen tissues of mice were plotted against the control group. B. Alu PCR analysis data of mouse blood, brain, heart, lung, liver, spleen, kidney, and gut tissues obtained from sacrifice 3 days after Jurkat/CAR T-cells injection.

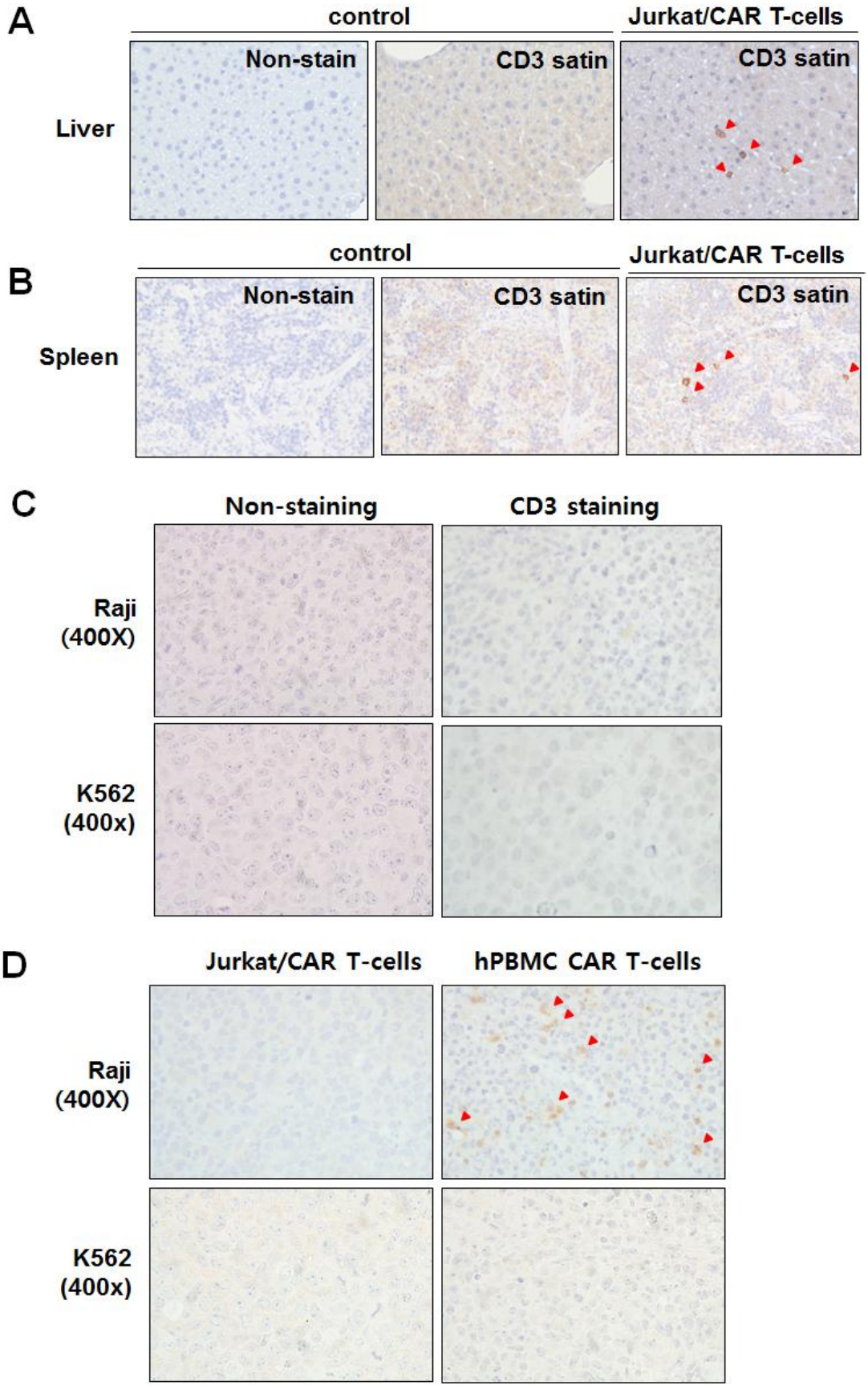
A
control
Jurkat/CAR T-cells
Non-stain
CD3 satin
CD3 satin
Liver
B
control
Jurkat/CAR T-cells
Non-stain
CD3 satin
CD3 satin
Spleen
C
Non-staining
CD3 staining
Raji
(400X)
K562
(400x)
D
Jurkat/CAR T-cells
hPBMC CAR T-cells
Raji
(400X)
K562
(400x)

Figure 8. IHC staining in mouse organs and tumors.

A. IHC staining with CD3 antibody demonstrates increased staining in liver tissue after Jurkat/CAR T-cells were injected into a mouse, compared to a control mouse liver. B. IHC staining with CD3 antibody demonstrates increased staining in spleen tissue after Jurkat/CAR T-cells were injected into a mouse, compared to control mouse spleen. Red arrows show CD3 targeting T-cells in IHC staining. C. IHC staining with CD3 antibody in Raji and K562 tumor tissues on day 3 after Jurkat/CAR T-cells injection. D. IHC staining with CD3 antibody in Raji and K562 tumor tissues on day 7 after Jurkat/CAR or hPBMC CAR T-cells injection. Red arrows show CD3 targeting T-cells in IHC staining.

국문 요약

배경: 최근 몇 년 사이에 키메라 항원 수용체 (chimeric antigen receptor, CAR) T-세포가 개발되어, 혈액학적 악성 종양 환자에 대한 임상 시험에서 극적인 효과를 나타냈다. 그러나, 주입한 CAR T-세포의 생체 내 거동을 추적하고 모니터링하기 위한 표준화된 방법은 없다. 본 연구는 양전자 방출 단층 촬영 (positron emission tomography, PET)을 이용하여 ^{89}Zr-p-Isothiocyanatobenzyl-desferrioxamine B (Df-Bz-NCS, DFO)가 표지된 CAR-T 세포를 추적하는 것이 가능한지 평가하고자 하였다.

방법: ^{89}Zr-DFO를 합성한 후, 10^6 세포 당 74～185 kBq을 사용하여 CD19을 표적으로 하는 CAR를 발현하는 Jurkat/CAR T-세포와 인간 말초혈액 단핵세포 (human peripheral blood mononuclear cell, hPBMC)로부터 유래한 CAR T-세포를 표지하였다. 세포 표지 효율을 얻었고, 방사성표지 세포들의 체외에서 세포 생존능, 증식능과 사이토카인 IL-2 혹은 IFN-γ 생산 기능을 비표지 대조군 세포들과 비교 평가하였다. CD19 양성 (Raji)과 음성 (K562) 림프종을 이종 이식한 마우스 모델을 개발하였고, ^{89}Zr-DFO 표지 된 Jurkat/CAR T-세포 또는 hPBMC CAR T-세포를 정맥주사 하여 양전자방출단층촬영(positron emission tomography, PET) 영상을 7일째까지 연속적으로 획득하였다. 모든 영상들은 정량 분석하였다. ^{89}Zr-DFO 표지 Jurkat/CAR T-세포의 최종 PET 영상 획득 후 동물을 희생하고 폐, 간 및 비장을 포함한 장기들을 분리하여 감마계수기로 계수하였다. 주입된 Jurkat/CAR T-cell의 분포는 유세포계측법, Alu-PCR 및 면역조직화학 염색법으로도 교차 확인하였다.

결과: Jurkat/CAR T-세포와 hPBMC CAR T-세포의 ^{89}Zr-DFO 표지효율은 70～79%이었고, 세포 방사성 표지 활성은 98.1 ~ 103.6 kBq/10^6세포였다. 세포 생존율은 95%이상이었다. 표지되지 않은 세포와 비교하여, 초기에는 세포 증식에 유의한 차이가 없었으나, 시간이 지남에 따라 증식능이 감소하였다 (p=0.02, 표지 7일 후). ^{89}Zr-DFO 표지 및 비표지 Jurkat/CAR T-세포의 Raji 세포에 대한 IL-2 분비는 유사하였고, ^{89}Zr-DFO 표지 후 hPBMC CAR T-세포의 IFN-γ의 생산도 표지 전과 유사하였다. PET 영상에서 ^{89}Zr-DFO 표지 Jurkat/CAR T-세포 주사 후 초기 1시간에는 대부분 폐(25.0% ± 3.7%ID)와 간(23.4% ± 5.3%ID)에 분포하였고, 이후 폐에 분포하던 세포들은 간으로 이동하고 이러한 분포는 7일째까지 비슷하게 유지되었다 (7일째: 폐 3.9% ± 1.0%ID, 간 35.7% ± 1.0%ID). 종양에서는 CD19 양성과 음성 종양 모두에서 유의한 CAR T-세포의 축적이 보이지 않았다. 비슷한 양상이 7일째에 생체 내 생체 분포에서 관찰되었다 (폐 3.0% ±1.0%ID, 간 19.8% ± 2.2 %ID, 비장 2.3% ± 1.7%ID). ^{89}Zr-DFO 표지 Jurkat/CAR T 및 hPBMC CAR T-세포의 생체 내 분포는 연속된 PET 이미지에서 유사한 패턴을 보였다. PET 영상에서 보인 Jurkat/CAR T-세포의 체내 분포는

유세포계측법, Alu-PCR 및 면역조직화학 염색법으로도 확인되었다.
결론: ^{89}Zr-DFO로 표지한 CAR T-세포의 체내 세포 주입 후 PET 영상을 이용하여 추적할 수 있는 가능성을 확인하였다. 이 결과는 ^{89}Zr-DFO 표지 CAR T-세포의 PET 영상기법이 향후 CAR T-세포 치료제 개발에서 세포 역학, 세포의 체내 초기 분포, 그리고 안전성을 파악하는데 이용될 수 있을 것이다.

중심단어: 키메라 항원 수용체 (CAR) T-세포, 세포 추적, p-Isothiocyanatobenzyl-desferrioxamine B (Df-Bz-NCS, DFO), 양전자방출단층촬영 (PET)